CMS Physics Analysis Summary

Contact: cms-pag-conveners-top@cern.ch 2014/05/17

Search for anomalous Wtb couplings and top FCNC in t-channel single-top-quark events

The CMS Collaboration

Abstract

Single-top-quark events in the t-channel are used to probe Wtb anomalous couplings and to search for top quark Flavor Changing Neutral Current (FCNC) interactions in proton-proton collisions at $\sqrt{s} = 7$ TeV. The analyzed data correspond to an integrated luminosity of 5 fb^{-1}. Events with the top quark decaying into a muon, neutrino and b-quark are selected. A Bayesian neural network is used to discriminate between signal and backgrounds. The observed event yields are consistent with SM prediction, and exclusion limits at 95% C.L. are determined. The exclusion limits on anomalous right vector and left tensor couplings of the Wtb vertex are found to be $|f_V^R| < 0.34$ and $|f_T^L| < 0.09$. In the scenarios with FCNC tcg and tug couplings, limits on the coupling strengths are found to be $\kappa_{tug}/\Lambda < 1.8 \cdot 10^{-2}$ TeV^{-1}, $\kappa_{tcg}/\Lambda < 5.6 \cdot 10^{-2}$ TeV^{-1} which corresponds to limits on the branching ratios $Br(t \to u + g) < 3.55 \times 10^{-4}$, $Br(t \to c + g) < 3.44 \times 10^{-3}$.

1 Introduction

The theory of electroweak interactions predicts three different production mechanisms for single-top-quarks in hadron-hadron collisions, in addition to the more abundant pair production due to the strong interaction. They are classified by the virtuality of the involved W boson [1] as t-, s-channel and associated tW-channel production.

The study of the single-top-quark production provides a possibility to investigate many aspects of top-quark physics that cannot be easily studied in $t\bar{t}$ production [2]. The three single-top-quark production channels are directly related to the squared modulus of the CKM matrix element V_{tb}, allowing for a direct measurement of this quantity and thus for a test of the standard model (SM). One can investigate the Wtb vertex structure and flavour changing neutral current (FCNC) couplings in the production and decay processes. The single-top-quark topologies provide a window for anomalous couplings and s-channel resonances like W' bosons. A review of the possible new physics scenarios to observe new physics from deviations in the expected cross sections of the t- and s-channel modes can be found in Ref. [3] and the references therein.

The t-channel production mechanism has the highest rate. We consider t-channel single-top-quark production as a signal process and estimate other single-top-quark production mechanisms as backgrounds. Only the muonic decay channel for the top quark is considered and μ + jets events are selected for the analysis.

We present the search for the anomalous Wtb couplings and for top-quark-gluon (tug or tcg) FCNC using the CMS 2011 data of proton-proton collisions at $\sqrt{s} = 7$ TeV. The separation between signal and background events is performed by means of a Bayesian Neural Network (BNN). The implementation of the BNN is done using the FBM package [4–6]. Limits on Wtb and top FCNC anomalous couplings are set from shape analysis of BNN discriminants using the Theta package [7, 8].

2 Data and Simulated Samples

The analysis is performed using the full accumulated 2011 data corresponding to 5 fb^{-1} at $\sqrt{s} = 7$ TeV proton-proton collision energy collected by the CMS experiment [9]. The production of t-channel single-top-quark is modeled by means of the CompHEP 4.5 package [10] with an additional method to simulate effective NLO approach [11]. The POWHEG generator [12] is used as an alternative model to estimate the sensitivity of our analysis to the signal modelling. Contributions of anomalous operators have been added to the CompHEP simulation for both the production and decay of top quarks, taking into account the top quark width, spin correlations between production and decay, and b-quark mass for the anomalous contribution as well as the SM contribution.

The MADGRAPH 5 [13] generator is used to simulate the main background processes; the top quark pair and the W-boson processes with up to 3 and 4 additionnal jets, respectively. The subdominant background processes are the production of Drell-Yan and di-bosons WW, WZ, ZZ, that have been modelled in PYTHIA 6 [14]. The contribution of multi-jet QCD processes, hereafter referred to as "QCD", is estimated using an orthogonal data sample. Additional samples were used in the analysis to estimate uncertainties due to variation of the factorization and renormalization scales and variation of matching parameters [15].

Table 1 includes the cross sections used for the normalization of simulated events. The quoted cross sections are from next-to-next-to-leading order calculations for the single top produc-

tion [16], pair top quark production [17], $W+$ jets [18] and other processes [19]. The statistical analysis of the Bayesian Neural Network output involves a reduction of the signal and background normalization uncertainties by means of nuisance parameters. This method significantly reduces the dependence of the analysis to the normalization. Due to the importance of the $W+$ jets background and the significant difference in kinematics, the following contributions are considered separately in the analysis: $W + QQ$ (a W boson produced together with a pair of b- or c-quarks), $W + c$ (a W boson produced in association with a c-quark), $W+$light quarks (events that do not contain heavy quarks) and $W + QX$ (events associated with underlying events, containing heavy quarks originating from the initial parton interaction). Different normalization scale factors for these components of the complete $W+$ jets MADGRAPH simulation were considered.

A reweighting procedure is applied on the simulation in order to reproduce the observed distribution of pile-up events. Additional small differences between data and the simulation of triggers and b-tagging are corrected by scale factors [20].

3 Event Selection

Electrons, muons, photons, charged and neutral hadron candidates are reconstructed and identified using the particle flow (PF) algorithm. Jets are defined by clustering PF particle candidates according to the anti-k_T algorithm with a cone size of 0.5. The production of t-channel single top quarks has the following signature: exactly one isolated charged lepton [21], one light-flavour jet in the forward region, one b-tagged jet [20] from the b quark originating from the decay of the top quark and an associated "soft" b-jet. The "soft" b-jet is likely to fail either the transverse momentum (p_{T}) threshold or the tracker acceptance. This channel is also characterized by significant missing transverse momentum ($E_{\mathrm{T}}^{\mathrm{miss}}$) due to the presence of a neutrino.

The following event selection (signal region) is therefore defined, restricting the analysis to the muon channel only:

- at least one primary vertex reconstructed from at least four tracks, with longitudinal (radial) distance of less than 24 (2) cm from the center of the detector;
- exactly one isolated (I^{μ}_{rel} <0.12) muon [21] with pseudorapidity $|\eta| < 2.1$ originating from the primary vertex, no additional muon or electrons passing looser quality criteria and $p_{\mathrm{T}} > 10$ (15 for electrons) GeV, $|\eta^{\mu}| < 2.5$, I^{μ}_{rel} <0.2; the relative isolation of the lepton I^{μ}_{rel} is defined as the sum of the energy deposited by stable charged hadrons, neutral hadrons and photons in a cone of size $\Delta R = \sqrt{(\Delta\eta^2 + \Delta\phi^2)} = 0.4$ around the charged lepton track, divided by its transverse momentum and $\eta = -\ln[\tan(\theta/2)]$;
- two or three jets with $p_{\mathrm{T}} > 30\,\mathrm{GeV}$ and the absolute value of the pseudorapidity $|\eta| < 4.7$;
- at least one b-quark tagged jet and at least one jet that fails the tight b-quark tagging working point (CSVT) [20].

The analysis is performed over the data collected with single-muon triggers. However, to accommodate the increasing instantaneous luminosity delivered by the LHC in 2011, different triggers were used for different data-taking periods and correspond to different thresholds of p_{T} threshold, ranging from 20 to 27 GeV. The described event selection corresponds to the signal region where the statistical analysis is performed. In addition, the control regions of events with 2 or 3 jets with no b-tagged jet and events with 4 jets 2 of which b-tagged are used to check

the modelling.

In the case of QCD-multijet production the reconstructed muons originate either from muons produced by the leptonic decay of heavy hadrons or from charged hadrons. As a result, these muon candidates are usually surrounded by hadronic activity. This feature is exploited to define a QCD control region by demanding exactly one muon with the inverted criteria of isolation from hadronic activity: $0.35 < I^{\mu}_{rel} < 1$. In order to better reproduce kinematics of the signal region, the jets falling inside a cone of size 0.5 around the selected muon are not considered in the analysis. The surviving jets are subject to the same selection as in the signal region.

To suppress QCD background we use a dedicated BNN. The following simple set of input variables sensitive to QCD is used: transverse mass of the reconstructed W boson [$M_T(W) = \sqrt{2p^{\mu}_T p^{\nu}_T (1 - cos(\phi_{\mu} - \phi_{\nu}))}$], the missing transverse energy $E^{\text{miss}}_{\text{T}}$, the transverse momentum of muons $p_T(\mu)$ and azimuthal angle $\Delta\phi(\mu, E^{\text{miss}}_{\text{T}})$ between muon and $E^{\text{miss}}_{\text{T}}$. In Fig. 1 data-to-simulation comparisons are shown for the QCD BNN discriminant and the $M_T(W)$ distribution. The QCD BNN discriminant and the transverse mass of the W boson demonstrate the agreement between data and simulation. The normalization of the QCD background is taken from a template fit to the QCD BNN distribution for the QCD model and all other processes involving a real W boson are normalized to their theoretical cross sections.

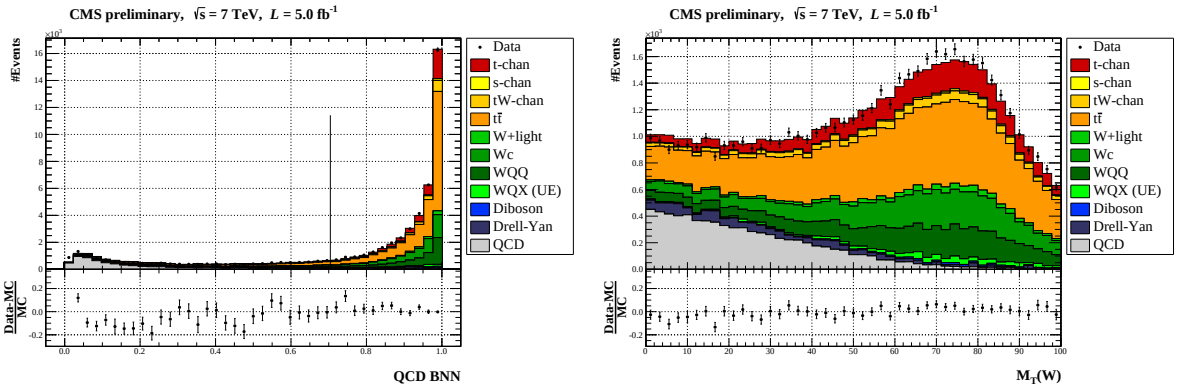

Figure 1: Discriminant used for the QCD-background rejection for the simulation and the data (left plot), and transverse W boson mass distribution (right plot), with statistical error bars only. The cut value is shown as a line on the left plot.

To reduce the QCD background, a cut on the QCD BNN discriminator of >0.7 is applied. Fig. 2 shows the performance of the QCD BNN for the training and testing events (left plot) and a comparison of cuts on QCD BNN discriminator and the $M_T(W)$ variable which is used in Ref. [22] (right plot). The events dedicated for the training of BNN are not used in the analysis.

A selection on the BNN rather than a selection on $M_T(W)$ allows to significantly increase the signal efficiency by 10%, while keeping a similar background rejection. With the cut on the QCD BNN about 90% of the QCD background is suppressed, while loosing only about 20% of signal events.

The event yields before and after the QCD background suppression and cross sections used for the MC normalization are listed in Table 1.

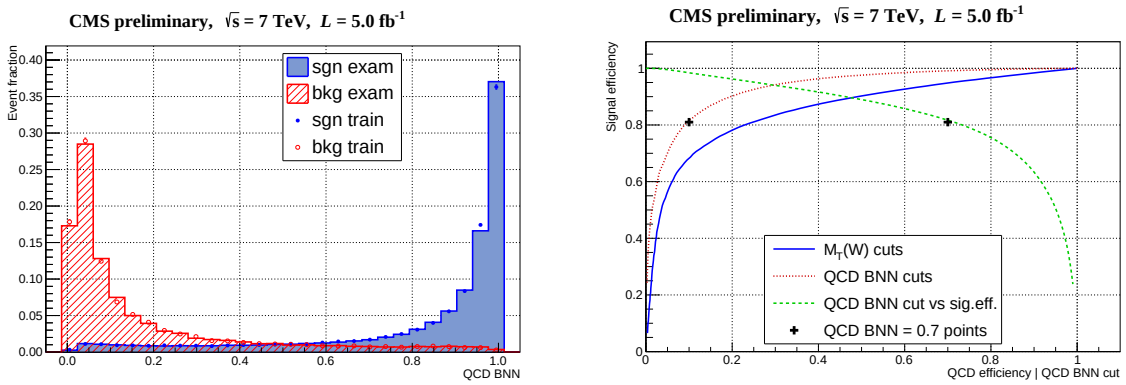

Figure 2: Separation power of the QCD BNN discriminator for the training ("train") and testing ("exam") events (left plot). Comparison of efficiencies of cuts for QCD background suppression. The blue curve shows efficiencies of $M_T(W)$ cuts, the red one of QCD BNN discriminator cuts. The green curve shows the signal efficiency w.r.t. to different QCD BNN cuts (right plot)

Process	Basic selection	QCD BNN > 0.7	Cross section
s-channel	$373.3^{+16.3}_{-14.5}$	$302.2^{+13.1}_{-11.8}$	$4.63^{+0.2}_{-0.18}$ pb [23]
tW-channel	$2079.0^{+154.5}_{-159.9}$	$1753.4^{+130.3}_{-134.8}$	$15.74^{+7.43}_{-7.69}$ pb [24]
$t\bar{t}$	$20750.1^{+778.1}_{-908.9}$	$17593.7^{+659.8}_{-770.6}$	$172.0^{+6.5}_{-7.6}$ pb [17]
W+jets	15286.1±761.2	12083.2±601.7	31314±1558 pb [18]
Diboson	378.4±13.6	300.8±10.9	67.1±1.7 pb [19]
Drell-Yan	1601.7±87.1	704.0±38.3	4998±272 pb [18]
QCD	7338.1	740.5	-
t-channel	$\mathbf{5563.1}^{+222.5}_{-161.9}$	$\mathbf{4545.5}^{+181.8}_{-132.3}$	$\mathbf{64.57}^{+2.58}_{-1.88}$ **pb** [25]
Simulation	$53369.9^{+1125.3}_{-1210.5}$	$38023.3^{+921.5}_{-996.6}$	
Data	56145	40681	

Table 1: The event yields for an integrated luminosity of 5 fb^{-1} before and after the QCD BNN cut. Cross sections used for the MC normalization and theoretical uncertainties are also shown.

4 Signal Extraction with Bayesian Neural Networks

Events that survive the initial selection and QCD BNN suppression are considered in the final analysis. The next step of the analysis is the preparation of the standard model BNN (SM BNN) to distinguish t-channel single top quark production from other SM processes. The tW-channel, $t\bar{t}$, W+jets, diboson and Drell-Yan processes are treated as a combined background for the SM BNN training. The SM BNN discriminant is used to separate SM backgrounds in the search for an anomalous structure at the Wtb vertex, where one more BNN (aWtb BNN) is prepared to separate anomalous contribution of right vector or left tensor couplings and that of the SM with left vector coupling. SM BNN and aWtb BNN discriminants are used together in the search for the deviations in the Wtb vertex. Two BNNs (tcg BNN and tug BNN) are trained to distinguish the corresponding couplings from SM contribution. The FCNC processes with anomalous tcg and tug vertices (vertices with the top quark, gluon and up/charm quark) are assumed to be completely independent of the SM contribution. The kinematic properties of any tcg and tug contributions are slightly different due to different initial state contributions and the discriminants of tcg BNN and tug BNN are used simultaneously in the statistical analysis to set 2D exclusion limits to the FCNC couplings.

During the preparation of BNNs the methods described in Ref. [26] are used for preprocessing and optimization, in particular of the renormalization of input variables, logarithmic scale

of the variables with long tails and of the BNN architecture. The event samples are divided into training and test subsamples. The samples used to train the BNN are not used further in the analysis. The choice of input variables for the BNNs is based on the Optimal Observables Method [27]. The method reflects the difference in the structure of Feynman diagrams contributing to signal and background processes. The BNN uses several variables as inputs, some of these require the full kinematic reconstruction of the top and the W candidates. For the reconstruction of the top quark mass the W-mass constraint is applied to extract the z component of neutrino. From the two real solutions of the equation the smallest one is chosen. For the events with an imaginary solution the imaginary component is eliminated by modifying $E_{\mathrm{T}}^{\mathrm{miss}}$ such that $M_T(W) = M_W$. Variables used for the SM BNN training are presented in Table 3.

The data-to-simulation comparisons (Fig. 3) show a good agreement in control regions enriched in top pair events (4 jets with 2 b-tags) and $W+$ jets (zero b-tag) as well as in the signal regions (Sec. 3). In Fig. 3 simulated events are normalized to theoretical cross sections and only statistical uncertainties are shown.

5 Systematic Uncertainties and Statistical Analysis

The aim of the statistical analysis is to extract the parameters of single top quark production and any signs of BSM behaviour based on the shapes of BNN discriminants. The analysis follows the same methodology for the estimation of the uncertainties as in the previously published measurements [22, 28]. Uncertainties considered in the analysis are discussed below.

For the variation of background normalization, scale parameters are introduced to the statistical model and the corresponding variation of these parameters are the same as for the SM measurement [22] and are listed in Table 2. All the background processes, and their normalization are treated as statistically independent.

Process	Uncertainty
top-quark pair production	15%
single top, s-channel	15%
single top, tW-channel	13%
W+jets, "WQQ"	100%
W+jets, "Wc"	100%
W+jets, "W+light"	50%
W+jets, "WQX (UE)"	50%
QCD (data-driven)	100%
Drell-Yan process	30%
WW, WZ, ZZ	30%

Table 2: Uncertainties on the background normalization

In order to estimate the uncertainty of the QCD template the different parameters of isolation criteria are used ($0.3< I^{\mu}_{rel} <0.5$ and $0.5< I^{\mu}_{rel} <1$), as well as the comparison with Monte-Carlo simulated events generated by PYTHIA. The considered deviations in the QCD template are covered by a conservative uncertainty of +100%/-50%, that is taken into account in the statistical analysis.

In order to estimate the uncertainties of jet energy resolution (JER), jet energy corrections (JEC) and $E_{\mathrm{T}}^{\mathrm{miss}}$ corrections, four-momenta of all reconstructed jets in simulated events are scaled simultaneously in accordance with (p_{T}, η)-dependent uncertainties of jet energy corrections [29].

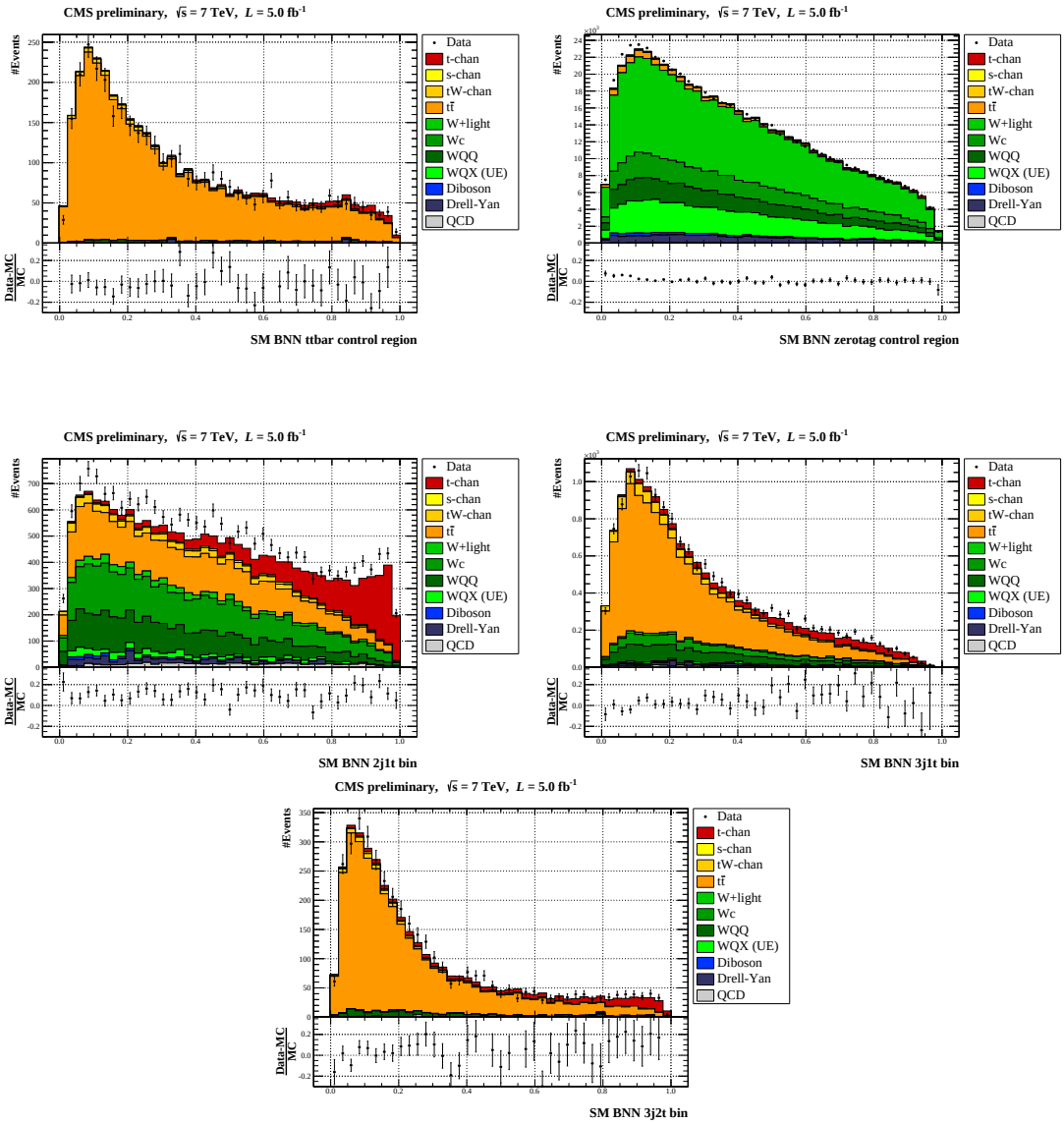

Figure 3: Data-to-simulation agreement of the SM BNN discriminant in the $t\bar{t}$ (4 jets with 1 tag) and $W+$ jets (no b-tagged jets) control regions, and in the signal region separated to three regions: two jets and one of them is b-tagged (2j1t), three jets and one of them is b-tagged (3j1t), three jets and two of them are b-tagged (3j2t). The simulation normalized to theoretical cross sections. The data points are shown with statistical error bars only.

Parameters of the procedure to correct jet energy resolution are varied within uncertainties and the procedure is repeated for all jets in simulation [30]. In addition to the impact of JEC and JER uncertainties on $E_{\mathrm{T}}^{\mathrm{miss}}$, an uncertainty on the unclustered component of $E_{\mathrm{T}}^{\mathrm{miss}}$ is evaluated.

The variations due to the uncertainty of b-quark tagging and mis-tagging efficiencies of jets are propagated in the form of additional weights to simulated events [20]. Uncertainty of the scale factors for c-quark jets is assumed to be twice as large as the uncertainty for b-quark jets. The scale factors for b- and c-quark jets are considered as totally correlated, whereas the mis-tagging scale factors are varied independently.

For the 2011 data-taking period, the luminosity was measured with a relative uncertainty of 2.2% [31].

The uncertainty of additional pp-interactions ("pile-up") is obtained by different pile-up multiplicity distributions obtained by changing the minimum bias cross-section by $\pm 5\%$.

The systematic uncertainty of the measured trigger scale factors includes variation of the invariant mass window of two muons ($[70, 110]$ GeV and $[50, 130]$ GeV) and systematic uncertainty due to the different trigger versions. A 3% systematic uncertainty is added to take the uncertainties of muon identification and isolation into account.

Uncertainty due to extra hard parton radiation and matching of the samples with different jet multiplicity is evaluated by doubling or halving the threshold for the MadGraph jet matching procedure for the top pair and W+jets production. Additional MadGraph samples have been generated with such shifts in the parameters.

The renormalization and factorization scale uncertainties are estimated with additional MC samples generated by doubling or halving the renormalization and factorization scales, for the signal and main background processes.

The uncertainty of the parton distribution functions (PDF) is evaluated by reweighting the simulated events according to the PDF4LHC recipe [32, 33]. According to the recommendation, uncertainties of three PDF sets are calculated and combined. We have found the uncertainty for the NNPDF set [34] is about two times higher than the MSTW set [35] and slightly higher than the CT10 set [36]. The PDF uncertainty is the dominant uncertainty in this analysis and is about 9%.

The uncertainty due to the choice of generator for the signal model is estimated using pseudo-data (i.e. the statistical model with all the parameters fixed by delta-functions). These pseudo-data are used to fit simulated events first with the CompHEP signal sample and then with the POWHEG signal sample. Half of the difference between these two measurements is taken as the uncertainty. This is a significant source of uncertainty found to be of the order of 5%.

Uncertainty due to finite statistics of the simulated samples is taken into account using the Barlow-Beeston method [37].

The BNN discriminator templates can be affected by different types of systematic uncertainties. Some of them are only changing the rate, while others change the shape. Shape and rate systematic uncertainties can be included in the statistical model by introducing additional nuisance parameters. The corresponding sources of marginalized uncertainty are JEC, JER, b-tagging, mistag rate, $E_{\mathrm{T}}^{\mathrm{miss}}$ and pile-up. This type of uncertainty is on the order of 6%. Some of the systematic uncertainties can not be implemented as nuisance parameters participating in the fit and can not be marginalized. The pseudo experiments are used to estimate un-marginalized uncertainties which are calculated as a shift of the corresponding fit from the nominal CompHEP result. The uncertainties which are considered as un-marginalized are: muon triggers, signal model, matching, renormalization and factorization scales and PDFs. The total un-marginalized uncertainty is about 11%.

In order to validate the analysis strategy and the statistical treatment of the uncertainties, we measure the cross section of the SM t-channel single top quark production. The measured value and uncertainty are in agreement with the previous measurement [22, 28] and with the prediction of SM.

The distribution of the SM BNN after the statistical analysis and evaluation of all the uncertainties are shown in Fig. 4, the hash band on the plot corresponds to the squared sum of marginalized and un-marginalized uncertainties.

6 Search for Anomalous Contributions to the Wtb Vertex

6.1 Anomalous Wtb vertex structure modelling

The single top quark t-channel is sensitive to the possible deviations from the SM predictions in the structure of the Wtb vertex. The most general, lowest dimension, CP conserving Lagrangian for the Wtb vertex has the following form [38, 39]:

$$\mathfrak{L} = -\frac{g}{\sqrt{2}}\bar{b}\gamma^{\mu}\left(f_V^L P_L + f_V^R P_R\right) tW_{\mu}^{-} - \frac{g}{\sqrt{2}}\bar{b}\frac{i\sigma^{\mu\nu}\partial_{\nu}W_{\mu}^{-}}{M_W}\left(f_T^L P_L + f_T^R P_R\right) t + h.c. \quad (1)$$

where $P_{L,R} = \frac{1\mp\gamma_5}{2}$, $\sigma_{\mu\nu} = \frac{i}{2}(\gamma_\mu\gamma_\nu - \gamma_\nu\gamma_\mu)$; form factor f_V^L (f_V^R) represents left (right) vector coupling, f_T^L (f_T^R) represents left (right) tensor coupling. The SM has the following set of coupling values: $f_V^L = V_{tb}, f_V^R = f_T^L = f_T^R = 0$, where V_{tb} is the CKM-matrix element. The same analysis scheme as in Ref. [40, 41] is used to look for possible deviations from SM: two of the four couplings are considered simultaneously (where one is always the left-vector coupling) and, accordingly, there are three scenarios: (f_V^L, f_V^R), (f_V^L, f_T^L) and (f_V^L, f_T^R). For each scenario the other two couplings are set to zero. The third scenario where the left vector and right tensor operators are both in the Wtb vertex is not considered in this study.

The kinematics and angular distributions significantly change in the presence of anomalous Wtb couplings, both in the production and in the decay of the top quark. Therefore it is important to correctly model the kinematics of the processes with anomalous couplings in the Wtb vertex. The anomalous Wtb couplings modelling is briefly described below. The technique is similar for both scenarios and is described here only for the (f_V^L, f_V^R) scenario.

For the (f_V^L, f_V^R) scenario, single top quark t-channel production cross-section is described by the expression:

$$\sigma = \left((f_V^L)^2 A_p + (f_V^R)^2 B_p\right) Br(t \to l, \nu, b) \quad (2)$$

and the branching fraction is of the following form: $Br(t \to l, \nu, b) = \left((f_V^L)^2 A_d + (f_V^R)^2 B_d\right)/w_{tot}$, where A_p, B_p (A_d, B_d) are some kinematic functions in the top quark production (decay) and w is the width of top quark. Thus the full expression for the cross-section is the following:

$$\sigma(f_V^L, f_V^R) = m(1000) + n(artificial) + k(0100) \quad (3)$$

where $m = \left(f_V^L\right)^4 \cdot w_{1000}/w_{tot}$, $n = \left(f_V^L\right)^2\left(f_V^R\right)^2 \cdot w_{art-0100}/w_{tot}$, $k = \left(f_V^R\right)^4 \cdot w_{0100}/w_{tot}$. The notation (1000), (artificial), (0100) corresponds to the kinematic terms factorized with the coupling value. The event samples which corresponds to the kinematic terms are simulated in CompHEP. The numbers in (1000), (0100) and (0010) notations are the coupling values in the order (f_V^L, f_V^R, f_T^L, f_T^R). For example, the SM sample corresponds to $f_V^L = V_{tb} \approx 1, f_V^R = 0$ values of the parameters and (1000) notation. The (artificial) event sample is simulated with the left vector coupling in the production and the right vector coupling in the decay of the top quark and vice versa. The full width as a function of f_V^L, f_V^R, f_T^L, f_T^R is given by [42]. All signal samples are simulated at the NLO precision with the technique from Ref. [11]

6.2 Exclusion limits on anomalous couplings

Following the strategy described in Sec. 4 in addition to the SM BNN, aWtb BNN is trained to distinguish the possible right vector structure and left vector structure in the t-channel single top quark events. The set of variables chosen for the BNN aWtb (f_V^L, f_V^R) is presented in Table 3. Fig. 5 shows the agreement between the data and simulation. The SM and aWtb BNN

discriminants are used as inputs in the statistical analysis of the 2D BNN discriminants. The results in the form of 2D exclusion limits are presented in Fig. 6. One-dimensional constraints on anomalous parameters were obtained by fixing one parameter to its SM value and setting the exclusion limit on the other one. The observed (expected) exclusion limits at 95 % C.L. are the following:

$$|f_V^L| > 0.90\ (0.88) \tag{4}$$
$$|f_V^R| < 0.34\ (0.39) \tag{5}$$

For the (f_V^L, f_T^L) scenario, another aWtb BNN is trained to separate the left-handed interacting single top quark events (SM) and the events with the left tensor operator in the Wtb vertex. Variables used for the training are presented in Table 3.

With these variables the aWtb BNN provides a good separation of events with the left tensor form factor in the Wtb interaction and events with SM kinematics. Data and model agreement for this discriminant is shown in Fig. 7.

The statistical analyses is performed to obtain the excluded regions at 68 and 95% C.L. for the couplings (f_V^L and f_T^L) (see Fig. 8).

As for the (f_V^L, f_V^R) scenario, one-dimensional constraints on anomalous parameters are obtained by fixing one parameter to its SM value and setting exclusion limit on the other one. The observed (expected) exclusion limits at 95 % C.L. are the following:

$$|f_V^L| > 0.92\ (0.88) \tag{6}$$
$$|f_T^L| < 0.09\ (0.16) \tag{7}$$

7 Search for tcg and tug FCNC anomalous couplings

7.1 Theoretical introduction

Interactions mediated by FCNC in the tcg and tug vertices may have significant strength. Such enhanced couplings are predicted by the models with multiple Higgs doublets, some classes of supersymmetric theories and models with the top quark as a composite particle [2]. FCNC tcg and tug interactions can be written in a model-independent form with the following vertex in the effective Lagrangian [2]:

$$\frac{\kappa_{tqg}}{\Lambda} g_s \overline{f} \sigma^{\mu\nu} \frac{\lambda^a}{2} t G^a_{\mu\nu} \tag{8}$$

where Λ is the scale of new physics $\mathcal{O}(1\ \text{TeV})$, $q = u(c)$ quark, κ_{tqg} defines the strength of the FCNC interactions in the tug or tcg vertices and $G^a_{\mu\nu}$ is a gauge tensor field of a gluon. The Lagrangian is assumed to be symmetric with respect to left and right projectors. The cross section of the single top quark production through FCNC is proportional to $(\kappa_{tqg}/\Lambda)^2$.

Single top quark production through FCNC contains 48 subprocesses (both for the u and c quark). The representative diagrams for FCNC tcg processes are presented in Fig. 9.

Similar processes defined by the exchange of the c quark to u quark, and the charge-conjugation processes, are also taken into account. The influence of the FCNC parameters on the total top quark width is negligible for the allowed region of FCNC parameters. Therefore the SM-value for the top quark width was used. The CompHEP generator was used for the simulation of the signal tug and tcg processes. All the FCNC samples are normalized to the NLO cross sections with a k-factor equal to 1.6 [43].

7.2 Exclusion limits on tug and tcg anomalous couplings

The search exploits the same signature as for the SM single top quark production processes, however the FCNC processes are kinematically different. Therefore it is reasonable to train a BNN for the discrimination of FCNC signal from the SM processes (with the SM t-channel single top quark production as a background). The difference with the SM analysis is the implementation of two BNNs instead of one BNN due to the possible presence of two signal FCNC tug and tcg processes.

The choice of variables for FCNC BNNs is motivated by the analysis of the Feynman diagrams of the signal and background processes and their kinematical properties. Input variables are presented in Table 3.

Two FCNC BNNs were trained separately; the first one for the FCNC tug and another one for the FCNC tcg processes. Data and model agreement of these networks is shown in Fig. 10.

Outputs of two FCNC BNNs with discrimination of FCNC tug(tcg) processes from the SM backgrounds were used as a basis for the statistical analysis. With the fit of histogram shapes and normalization, the posterior distributions of κ_{tug}/Λ and κ_{tcg}/Λ are obtained. The 2D contour of FCNC parameters is shown in Fig. 11.

Individual exclusion limits on κ_{tug}/Λ are obtained by fixing κ_{tcg}/Λ to zero and vice versa. The observed (expected) exclusion limits at 95 % C.L. are the following:

$$\frac{\kappa_{tug}}{\Lambda} < 1.8 \cdot 10^{-2}\ (1.2 \cdot 10^{-2})\ \text{TeV}^{-1}, \tag{9}$$

$$\frac{\kappa_{tcg}}{\Lambda} < 5.6 \cdot 10^{-2}\ (3.1 \cdot 10^{-2})\ \text{TeV}^{-1}. \tag{10}$$

In terms of branching fractions [44]:

$$Br(t \rightarrow u + g) < 3.55 \times 10^{-4}\ (1.58 \times 10^{-4}), \tag{11}$$

$$Br(t \rightarrow c + g) < 3.44 \times 10^{-3}\ (1.05 \times 10^{-3}) \tag{12}$$

8 Conclusion

Direct search of new physics were performed in the single-top-quark production processes in the t-channel. The analysis considers model-independent anomalous operators in the Wtb vertex and tcg/tug FCNC couplings. Different scenarios are considered for the anomalous contributions. The observed event yields are consistent with SM prediction, and exclusion limits at 95% C.L. are determined. The exclusion limits on the possible Wtb anomalous couplings are measured to be $|f_V^R| < 0.34$ for the right vector coupling and $|f_V^T| < 0.09$ for the left tensor coupling. In the scenario with FCNC tug and tcg couplings, the exclusion limits on the coupling strengths are $k_u/\Lambda < 1.8 \cdot 10^{-2}$ TeV^{-1}, $k_c/\Lambda < 5.6 \cdot 10^{-2}$ TeV^{-1} or in terms of branching fractions $Br(t \rightarrow u + g) < 3.55 \times 10^{-4}$, $Br(t \rightarrow c + g) < 3.44 \times 10^{-3}$. Exclusion limits with simultaneous variation of the couplings are also provided.

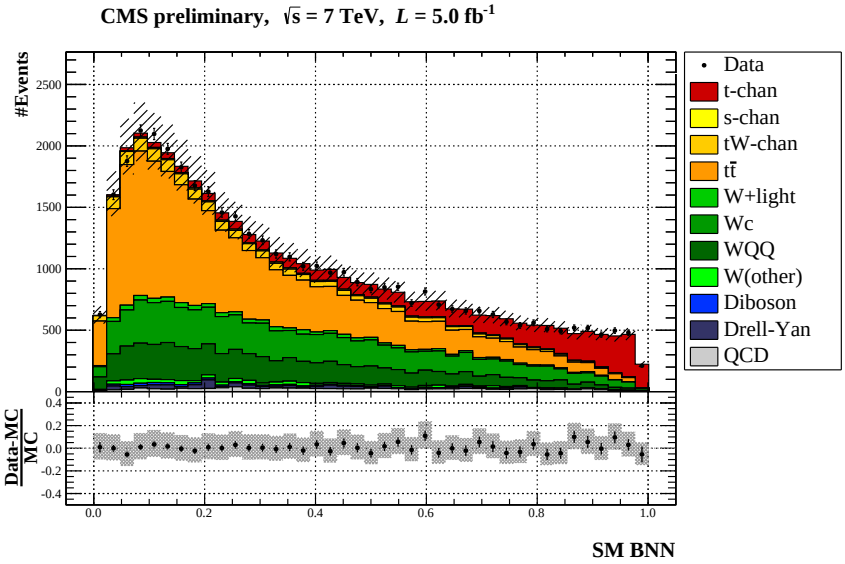

Figure 4: The SM BNN discriminant after the statistical analysis and evaluation of all the uncertainties. The hashed band corresponds to the systematic uncertainty. The points in the ratio plot are shown with statistical errors only.

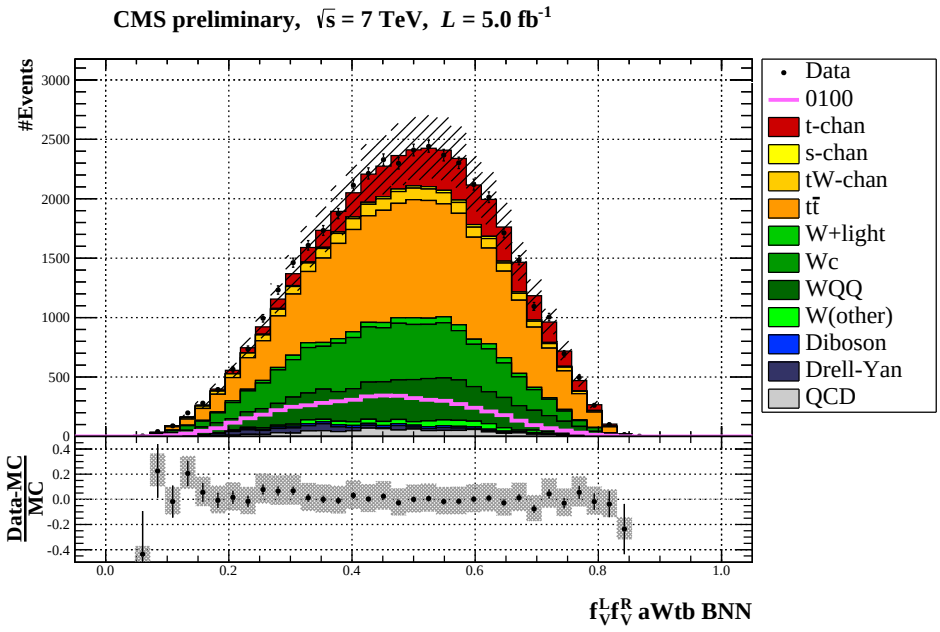

Figure 5: Data and model comparison of BNN anomalous Wtb discriminator for the (f_V^L, f_V^R) scenario. The BNN aWtb was trained to separate events with right-handed vector operator in the Wtb interaction and SM single top quark. The hashed band corresponds to systematic uncertainty.

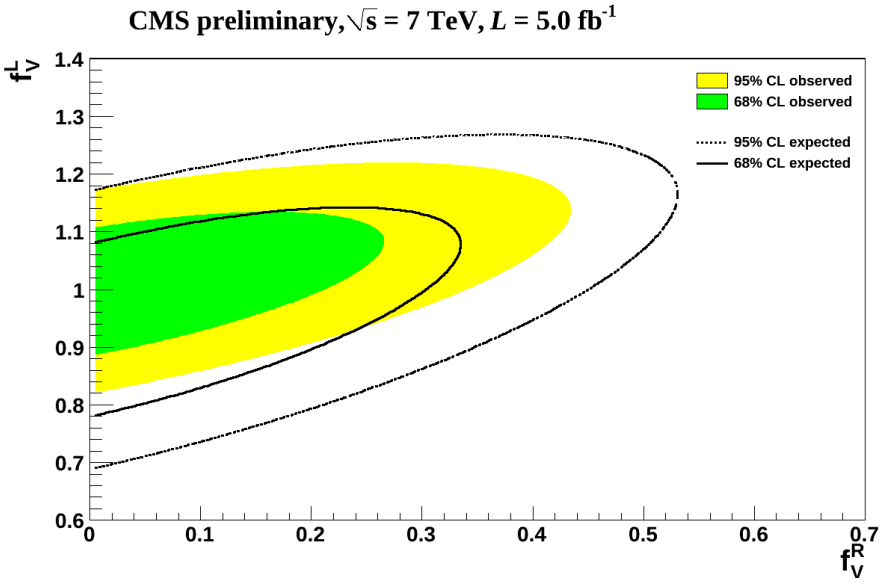

Figure 6: Exclusion limits in two-dimensions on $(f_V^L,\ f_V^R)$-couplings at 68% and 95% C.L. for the observed and expected limits.

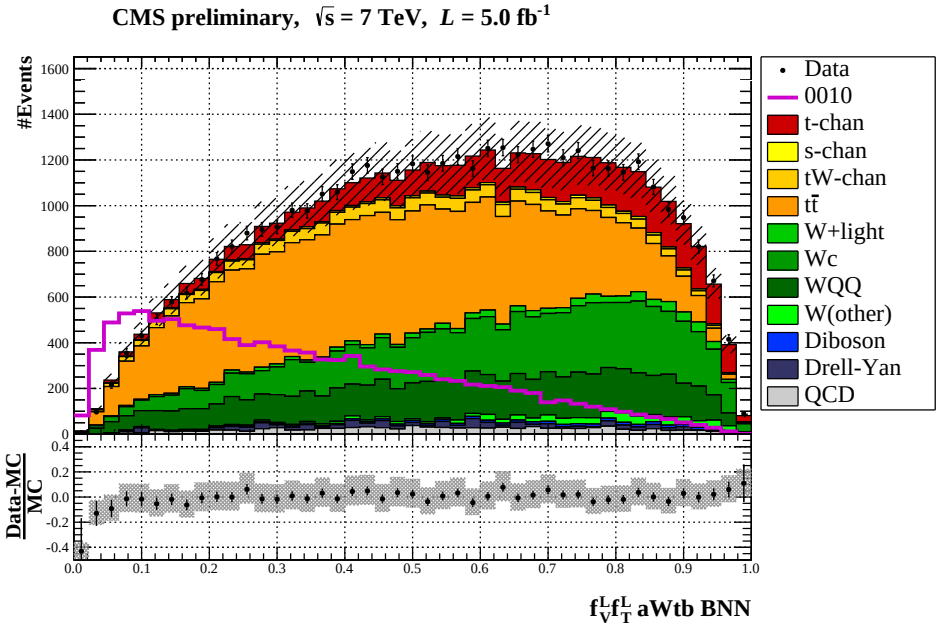

Figure 7: Data and model comparison of BNN aWtb discriminant for the $(f_V^L,\ f_T^L)$ scenario. The BNN aWtb was trained to separate possible events with left tensor coupling in the Wtb interaction and SM events. The hashed band corresponds to the systematic uncertainty.

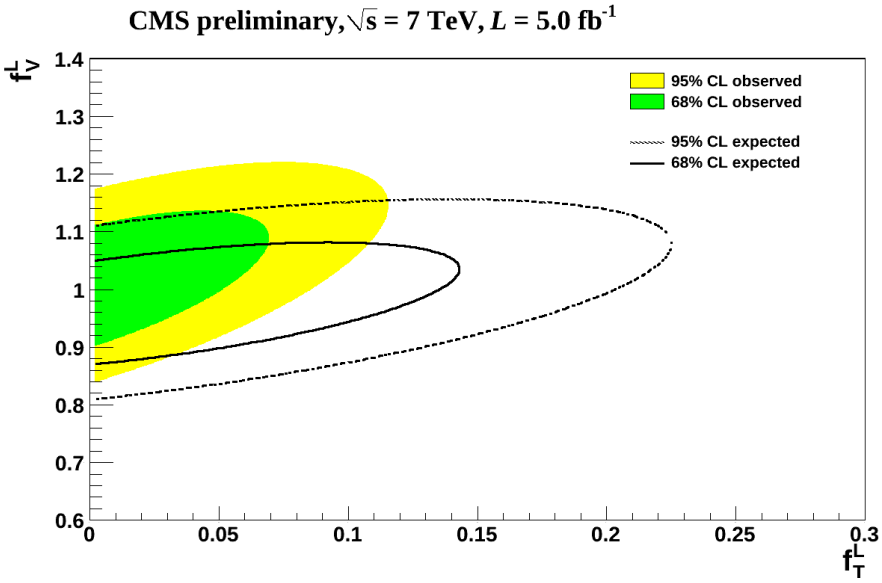

Figure 8: Exclusion limits in two-dimensions on (f_V^L, f_T^L)-couplings at 68% and 95% C.L. for the observed and expected limits.

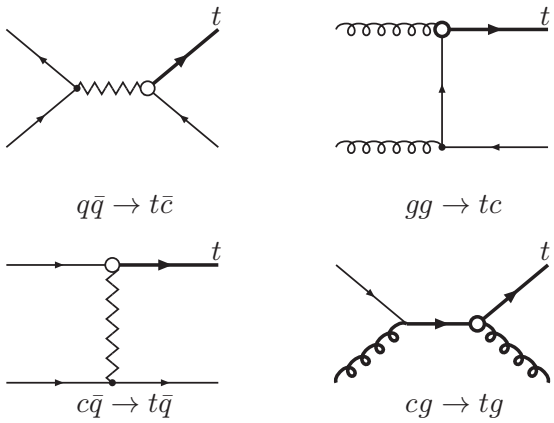

Figure 9: Representative Feynman diagrams for FCNC tcg processes; the diagrams for FCNC tug processes are similar.

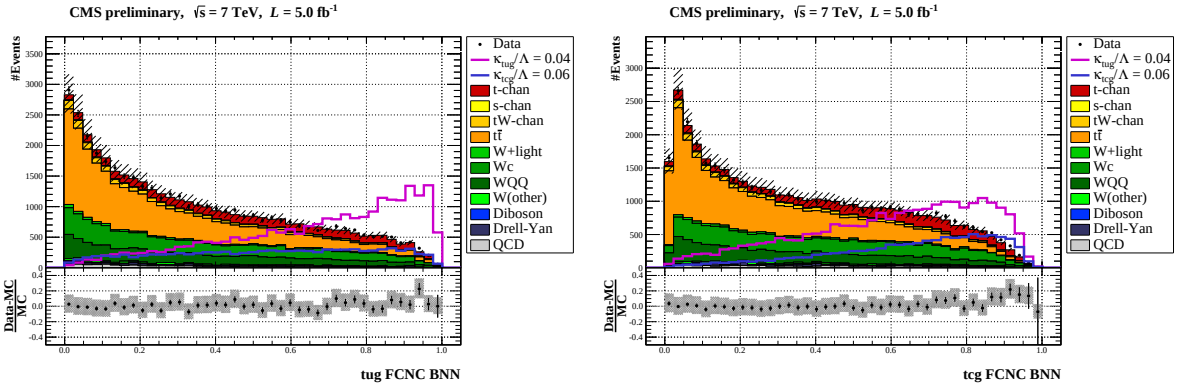

Figure 10: Data and model agreement for the FCNC BNN discriminants. The tug/tcg FCNC BNNs are trained to separate tug/tcg events from all SM processes. The hashed band corresponds to systematic uncertainty.

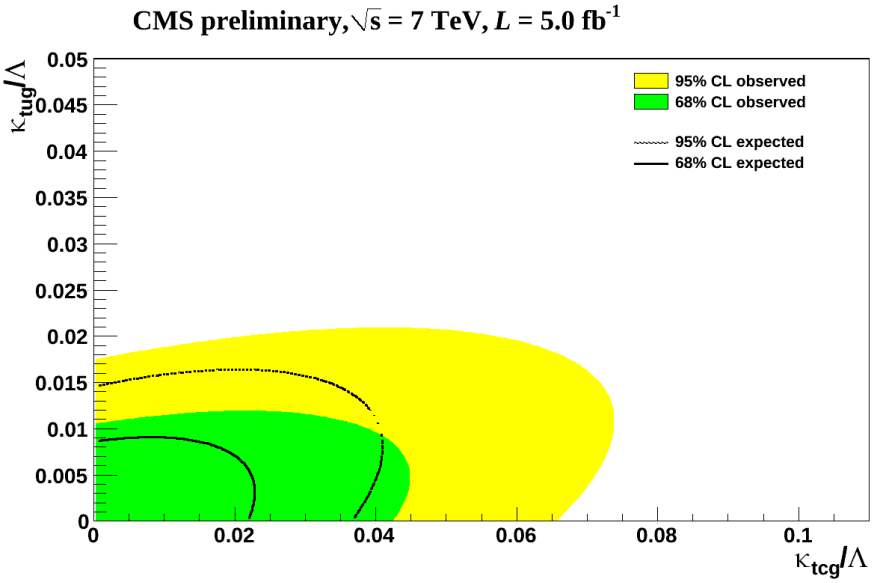

Figure 11: Exclusion upper limits in two-dimensions on $\frac{\kappa_{tug}}{\Lambda}$, $\frac{\kappa_{tcg}}{\Lambda}$-couplings at 68% and 95% C.L.

Variable	Description	SM BNN	$f_V^L f_V^R$ BNN	$f_V^L f_T^L$ BNN	tug BNN	tcg BNN
$p_{\mathrm{T}}(b_1)$	p_T of the leading-b-jet (the b-tagged jet with the highest p_T) — hereinafter we use the notations "leading" and "second-leading" for jets correspondingly to their order in p_T, the decreasing one	V		V	V	V
$p_{\mathrm{T}}(b_2)$	p_T of the second-leading b-jet	V				V
$p_{\mathrm{T}}(j_1 j_2)$	a vector sum of p_T of the first and the second-leading jets	V		V	V	V
$p_{\mathrm{T}}(\sum_{i \neq i_{best}} \vec{p_T}(j_i))$	a vector sum of p_T of all jets without the best jet. The notation "best jet" is used for the jet which gives the invariant mass of the top quark closest to the value of 172.5 GeV, which is used in the MC simulation	V			V	V
$p_{\mathrm{T}}(j_L)$	p_T of the light-flavour jet (untagged jet with the highest value of $\lvert\eta\rvert$)	V			V	V
$p_{\mathrm{T}}(\mu)$	transverse momenta of the muon	V	V	V		V
$p_{\mathrm{T}}(W, b_1)$	p_T of the W boson and the leading-b-jet	V		V	V	V
$p_{\mathrm{T}}(W)$	p_T of the W boson				V	V
H_T	scalar sum of p_T of all jets			V		
$E_{\mathrm{T}}^{\mathrm{miss}}$	missing transverse energy (energy of the reconstructed neutrino)		V			V
$\eta(\mu)$	η of the muon	V			V	V
$\eta(j_L)$	η of the light-flavour jet	V		V	V	V
$M(j_1 j_2)$	the invariant mass of the leading-jet and the second-leading jets	V		V		
$M(\sum_{i \neq i_{best}}(j_i))$	the invariant mass of all jets without the best one	V				V
$M(jW)$	the invariant mass of the W boson and all jets	V				
$M(W, b_1)$	the invariant mass of the W boson and the leading-b-jet	V			V	V
$M(\sum_i(j_i))$	the invariant mass of all jets				V	V
$\Delta R(j_1, j_2)$	equal to $\sqrt{(\eta(j_1)-\eta(j_2))^2+(\phi(j_1)-\phi(j_2))^2}$	V			V	V
$\Delta R(\mu, j_2)$	equal to $\sqrt{(\eta(\mu)-\eta(j2))^2+(\phi(\mu)-\phi(j2))^2}$			V		
$\Delta\phi(\mu, E_{\mathrm{T}}^{\mathrm{miss}})$	azimuthal angle between the lepton and the reconstructed neutrino			V	V	V
$cos(\theta_{\mu,j_L})\lvert_{top}$	the cosine of the angle between the lepton and the light flavour jet in the top quark rest frame, the top quark is reconstructed with the leading-b-jet [45]	V	V		V	V
$cos(\theta_{\mu,W})\lvert_W$	the cosine of the angle between the lepton and the W boson in the W boson rest frame [46]		V	V	V	V
$cos(\theta_{W,j_L})\lvert_{top}$	the cosine of the angle between the W boson and the light-flavour jet in the top quark rest frame [46]		V			
$cos(\theta_{\mu,j_1})\lvert_{top}$	the cosine of the angle between the lepton and the first jet in the top quark rest frame					V
$Q(\mu)$	a charge of the lepton				V	V

Table 3: Input variables of BNNs used in the analysis. Sign V marks the variables used for the particular BNN.

References

[1] S. S. Willenbrock and D. A. Dicus, "Production of Heavy Quarks from W Gluon Fusion", *Phys.Rev.* **D34** (1986) 155, doi:10.1103/PhysRevD.34.155.

[2] M. Beneke et al., "Top quark physics", arXiv:hep-ph/0003033.

[3] E. Boos and L. Dudko, "The Single Top Quark Physics", *Int.J.Mod.Phys.* **A27** (2012) 1230026, doi:10.1142/S0217751X12300268, arXiv:1211.7146.

[4] R. M. Neal, "Bayesian Learning for Neural Networks", Technical Report ISBN 0-387-94724-8, Dept. of Statistics and Dept. of Computer Science, University of Toronto, 1994.

[5] R. M. Neal, "Software for Flexible Bayesian Modeling and Markov Chain Sampling", Technical Report 2004-11-10, Dept. of Statistics and Dept. of Computer Science, University of Toronto, 2004.

[6] P. Bhat and H. Prosper, "Bayesian neural networks", *Conf.Proc.* **C050912** (2005) 151–154.

[7] Th. Müller, J. Ott, and J. Wagner-Kuhr, "theta — A Framework for Template-Based Modeling and Inference", technical report, 2010. CMS-IN-2010/017 (internal).

[8] Th. Müller, J. Ott, and J. Wagner-Kuhr, "http://www-ekp.physik.uni-karlsruhe.de/~ott/theta/html/index.html", technical report.

[9] CMS Collaboration, "The CMS experiment at the CERN LHC", *JINST* **0803** (2008) S08004, doi:10.1088/1748-0221/3/08/S08004.

[10] E. Boos et al., "CompHEP 4.4: Automatic computations from Lagrangians to events", *Nucl.Instrum.Meth.* **A534** (2004) 250–259, doi:10.1016/j.nima.2004.07.096, arXiv:hep-ph/0403113.

[11] E. Boos et al., "Method for simulating electroweak top-quark production events in the NLO approximation: SingleTop event generator", *Phys.Atom.Nucl.* **69** (2006) 1317–1329, doi:10.1134/S1063778806080084.

[12] S. Alioli, P. Nason, C. Oleari, and E. Re, "A general framework for implementing NLO calculations in shower Monte Carlo programs: the POWHEG BOX", *JHEP* **06** (2010) 043, doi:10.1007/JHEP06(2010)043, arXiv:1002.2581.

[13] J. Alwall et al., "MadGraph 5 : Going Beyond", *JHEP* **1106** (2011) 128, doi:10.1007/JHEP06(2011)128, arXiv:1106.0522.

[14] T. Sjöstrand, S. Mrenna, and P. Z. Skands, "PYTHIA 6.4 Physics and Manual", *JHEP* **0605** (2006) 026, doi:10.1088/1126-6708/2006/05/026, arXiv:hep-ph/0603175.

[15] J. Alwall, S. de Visscher, and F. Maltoni, "QCD radiation in the production of heavy colored particles at the LHC", *JHEP* **0902** (2009) 017, doi:10.1088/1126-6708/2009/02/017, arXiv:0810.5350.

[16] N. Kidonakis, "Differential and total cross sections for top pair and single top production", arXiv:1205.3453.

[17] M. Czakon, P. Fiedler, and A. Mitov, "Total Top-Quark Pair-Production Cross Section at Hadron Colliders Through $O(\frac{4}{S})$", *Phys.Rev.Lett.* **110** (2013), no. 25, 252004, doi:10.1103/PhysRevLett.110.252004, arXiv:1303.6254.

[18] R. Gavin, Y. Li, F. Petriello, and S. Quackenbush, "FEWZ 2.0: A code for hadronic Z production at next-to-next-to-leading order", arXiv:1011.3540.

[19] J. M. Campbell and R. Ellis, "MCFM for the Tevatron and the LHC", *Nucl.Phys.Proc.Suppl.* **205-206** (2010) 10–15, doi:10.1016/j.nuclphysbps.2010.08.011, arXiv:1007.3492.

[20] CMS Collaboration, "Identification of b-quark jets with the CMS experiment", *JINST* **8** (2013) 04013, doi:10.1088/1748-0221/8/04/P04013, arXiv:1211.4462.

[21] CMS Collaboration, "Performance of CMS muon reconstruction in pp collision events at $\sqrt{s} = 7$ TeV", *JINST* **7** (2012) P10002, doi:10.1088/1748-0221/7/10/P10002, arXiv:1206.4071.

[22] CMS Collaboration, "Measurement of the single-top-quark t-channel cross section in pp collisions at $\sqrt{s} = 7$ TeV", *JHEP* **1212** (2012) 035, doi:10.1007/JHEP12(2012)035, arXiv:1209.4533.

[23] N. Kidonakis, "NNLL resummation for s-channel single top quark production", *Phys.Rev.* **D81** (2010) 054028, doi:10.1103/PhysRevD.81.054028, arXiv:1001.5034.

[24] N. Kidonakis, "Two-loop soft anomalous dimensions for single top quark associated production with a W- or H-", *Phys.Rev.* **D82** (2010) 054018, doi:10.1103/PhysRevD.82.054018, arXiv:1005.4451.

[25] N. Kidonakis, "Next-to-next-to-leading-order collinear and soft gluon corrections for t-channel single top quark production", *Phys.Rev.* **D83** (2011) 091503, doi:10.1103/PhysRevD.83.091503, arXiv:1103.2792.

[26] E. Boos et al., "Optimization of the analysis of single top-quark production at the Large Hadron Collider (LHC)", *Phys.Atom.Nucl.* **73** (2010) 971–984, doi:10.1134/S1063778810060116.

[27] E.Boos et al., "Method of Optimum Observables and Implementation of Neural Networks in Physics Investigations", *Phys. Atom. Nucl.* **71** (2008) 383–393.

[28] CMS Collaboration, "Measurement of the t-channel single top quark production cross section in pp collisions at $\sqrt{s} = 7$ TeV", *Phys.Rev.Lett.* **107** (2011) 091802, doi:10.1103/PhysRevLett.107.091802, arXiv:1106.3052.

[29] CMS Collaboration, "Determination of jet energy calibration and transverse momentum resolution in CMS", *JINST* **6** (2011) 11002, doi:10.1088/1748-0221/6/11/P11002, arXiv:1107.4277.

[30] CMS Collaboration, "Jet energy resolution in CMS at $\sqrt{s} = 7$ TeV", CMS Physics Analysis Summary JME-10-014, 2010.

[31] CMS Collaboration, "Absolute calibration of the luminosity measurement at CMS: Winter 2012 update", CMS Physics Analysis Summary SMP-12-008, 2012.

[32] S. Alekhin et al., "The PDF4LHC Working Group Interim Report", arXiv:1101.0536.

[33] M. Botje et al., "The PDF4LHC Working Group Interim Recommendations", arXiv:1101.0538.

[34] R. D. Ball et al., "Parton distributions with LHC data", *Nucl.Phys.* **B867** (2013) 244–289, doi:10.1016/j.nuclphysb.2012.10.003, arXiv:1207.1303.

[35] A. Martin, W. Stirling, R. Thorne, and G. Watt, "Parton distributions for the LHC", *Eur.Phys.J.* **C63** (2009) 189–285, doi:10.1140/epjc/s10052-009-1072-5, arXiv:0901.0002.

[36] J. Gao et al., "The CT10 NNLO Global Analysis of QCD", *Phys.Rev.* **D89** (2014) 033009, doi:10.1103/PhysRevD.89.033009, arXiv:1302.6246.

[37] R. Barlow, "Fitting using finite Monte Carlo samples", *Computer Physics Communications* **77** (1993) 219228.

[38] W. Buchmuller and D. Wyler, "Effective Lagrangian Analysis of New Interactions and Flavor Conservation", *Nucl.Phys.* **B268** (1986) 621, doi:10.1016/0550-3213(86)90262-2.

[39] G. L. Kane, G. Ladinsky, and C. Yuan, "Using the Top Quark for Testing Standard Model Polarization and CP Predictions", *Phys.Rev.* **D45** (1992) 124–141, doi:10.1103/PhysRevD.45.124.

[40] D0 Collaboration, "Search for anomalous Wtb couplings in single top quark production", *Phys.Rev.Lett.* **101** (2008) 221801, doi:10.1103/PhysRevLett.101.221801, arXiv:0807.1692.

[41] D0 Collaboration, "Search for anomalous Wtb couplings in single top quark production in $p\bar{p}$ collisions at $\sqrt{s} = 1.96$ TeV", *Phys.Lett.* **B708** (2012) 21–26, doi:10.1016/j.physletb.2012.01.014, arXiv:1110.4592.

[42] M. Mohammadi Najafabadi, "Secondary particles spectra in decay of polarized top quark with anomalous tWb coupling", *J.Phys.* **G34** (2007) 39–46, doi:10.1088/0954-3899/34/1/003, arXiv:hep-ph/0601155.

[43] J. J. Liu, C. S. Li, L. L. Yang, and L. G. Jin, "Next-to-leading order QCD corrections to the direct top quark production via model-independent FCNC couplings at hadron colliders", *Phys.Rev.* **D72** (2005) 074018, doi:10.1103/PhysRevD.72.074018, arXiv:hep-ph/0508016.

[44] J. J. Zhang et al., "Next-to-leading order QCD corrections to the top quark decay via model-independent FCNC couplings", *Phys.Rev.Lett.* **102** (2009) 072001, doi:10.1103/PhysRevLett.102.072001, arXiv:0810.3889.

[45] G. Mahlon and S. J. Parke, "Improved spin basis for angular correlation studies in single top quark production at the Tevatron", *Phys.Rev.* **D55** (1997) 7249–7254, doi:10.1103/PhysRevD.55.7249, arXiv:hep-ph/9611367.

[46] J. Aguilar-Saavedra and R. Herrero-Hahn, "Model-independent measurement of the top quark polarisation", *Phys.Lett.* **B718** (2012) 983–987, doi:10.1016/j.physletb.2012.11.031, arXiv:1208.6006.